INPP5K and SIL1 associated pathologies with overlapping clinical phenotypes converge through dysregulation of PHGDH

Denisa Hathazi,[1,2,†] Dan Cox,[3,†] Adele D'Amico,[4,‡] Giorgio Tasca,[5,‡] Richard Charlton,[3] Robert-Yves Carlier,[6,7] Jennifer Baumann,[1] Laxmikanth Kollipara,[1] René P. Zahedi,[1,8] Ingo Feldmann,[1] Jean-Francois Deleuze,[9] Annalaura Torella,[10] Ronald Cohn,[11] Emily Robinson,[12] Francesco Ricci,[12] Heinz Jungbluth,[13] Fabiana Fattori,[4] Anne Boland,[9] Emily O'Connor,[14] Rita Horvath,[2] Rita Barresi,[3] Hanns Lochmüller,[14,15] Andoni Urtizberea,[16] Marie-Line Jacquemont,[17] Isabelle Nelson,[18] Laura Swan,[12] Gisèle Bonne[18,‡] and Andreas Roos[13,19,‡]

[†,‡]**These authors contributed equally to this work.**

Abstract

Marinesco-Sjögren syndrome (MSS) is a rare human disorder caused by biallelic mutations in *SIL1* characterized by cataracts in infancy, myopathy and ataxia, symptoms that are also associated with a novel disorder caused by mutations in *INPP5K*. While these phenotypic similarities may suggest commonalties at a molecular level, an overlapping pathomechanism has not been established yet. In this study, we present six new INPP5K patients and expand the current mutational and phenotypical spectrum of the disease showing the clinical overlap between MSS and the INPP5K-phenotype. We applied unbiased proteomic profiling on cells derived from MSS- and INPP5K-patients and identified alterations in D-3-phosphoglycerate dehydrogenase as a common molecular feature. D-3-phosphoglycerate dehydrogenase modulates the production of L-serine and mutations in this enzyme were previously associated with a neurological phenotype, which clinically overlaps with MSS and INPP5K-disease. As, L-serine administration represents a promising therapeutic strategy for D-3-phosphoglycerate dehydrogenase patients, we tested the effect of L-serine in generated *sil1*, *phgdh* and *inpp5k a+b* zebrafish models which showed an improvement in their neuronal phenotype. Thus our study defines a core phenotypical feature underpinning a

key common molecular mechanism in three rare diseases and reveals a common and novel therapeutic target for these patients.

Author affiliations:

1 Leibniz-Institut für Analytische Wissenschaften - ISAS - e.V, Dortmund, Germany

2 Department of Clinical Neurosciences, School of Clinical Medicine, University of Cambridge, Cambridge, UK

3 The John Walton Muscular Dystrophy Research Centre, Translational and Clinical Research Institute, Faculty of Medical Sciences, Newcastle University, International Centre for Life, Newcastle upon Tyne, UK

4 Laboratory of Molecular Medicine for Neuromuscular and Neurodegenerative Disorders, Bambino Gesù Children's Hospital, Rome Italy

5 Unità Operativa Complessa di Neurologia, Fondazione Policlinico Universitario A. Gemelli IRCCS, Rome, Italy

6AP-HP, Service d'Imagerie Médicale, Raymond Poincaré Hospital, Garches, France

7 Inserm U 1179, University of Versailles Saint-Quentin-en-Yvelines (UVSQ), Versailles, France

8 Segal Cancer Proteomics Centre, Lady Davis Institute, Jewish General Hospital, McGill University, Montreal, Canada

9 Centre National de Recherche en Génomique Humaine (CNRGH) (A.B., J.F.D.), Institut de Biologie François Jacob, CEA, Université Paris-Saclay, Evry, France

10 Dipartimento di Medicina di Precisione, Università degli Studi della Campania "Luigi Vanvitelli", Naples, Italy and Telethon Institute of Genetics and Medicine, Pozzuoli, Italy

11 SickKids Research Institute, Department of Paediatrics and Molecular Genetics, University of Toronto, Toronto, Canada

12 Department of molecular Physiology and Cell Signalling, Institute of Systems, Molecular and Integrative Biology, University of Liverpool, Crown Street, Liverpool, UK

13 Guy's and St Thomas' NHS Trust and King's College London, London, UK

14 Children's Hospital of Eastern Ontario Research Institute, University of Ottawa, Ottawa, Canada

15 Department of Neuropediatrics and Muscle Disorders, Medical Center - University of Freiburg, Faculty of Medicine, Freiburg, Germany

16 Hôpital Marin de Hendaye, Hendaye, France

17 Unité de Génétique Médicale, Pôle Femme-Mère-Enfant, Groupe Hospitalier Sud Réunion, CHU de La Réunion, La Réunion, France

18 Sorbonne Université, Inserm UMRS974, Centre de Recherche en Myologie, Institut de Myologie, Paris, France

19 Department of Pediatric Neurology, University Hospital Essen, University of Duisburg-Essen, Faculty of Medicine, Essen, Germany

Correspondence to: Andreas Roos, PhD

Pediatric Neurology, University of Duisburg-Essen, Faculty of Medicine, Essen, Germany

E-mail: andreas.roos@uk-essen.de

Running title: Molecular linkage between MSS and MSS-like phenotype

Keywords: SIL1; BiP; PHGDH; INPP5K; L-serine

INTRODUCTION:

Muscle diseases may be complicated with additional clinical hallmarks such as abnormalities of the eye, intellectual disability and neurodegeneration, leading to syndromic disorders. Marinesco-Sjögren syndrome (MSS) is an autosomal recessive disorder with infantile onset cataracts, cerebellar atrophy, microcephaly, intellectual disability (of varying degree) and progressive muscle wasting due to vacuolar myopathy [1-3]. Marinesco-Sjögren syndrome (MSS) is an autosomal

recessive disorder with an infantile onset featuring cataracts, cerebellar atrophy, intellectual disability (of varying degree), microcephaly and progressive muscle wasting due to vacuolar myopathy [1-3]. MSS is caused by mutations in the *SIL1* gene [4-6], which encodes a co-chaperone known as nucleotide exchange factor SIL1. This protein facilitates the efficient cycling of ADP and ATP for GRP78/BiP, one of the main chaperones of the endoplasmic reticulum [7]. Recently, recessive missense mutations in the *INPP5K* gene were linked to a new syndromic childhood onset neuromuscular disease [8, 9]. So far, the p.Ile50Thrmutation affecting the 5-phosphatase domain of INPP5K seems to represent the most frequent pathogenic amino acid substitution [8]. INPP5K, a skeletal muscle and kidney enriched inositol phosphatase acts as a $PI(4,5)P_2$ phosphatase and regulates the actin cytoskeleton, insulin signalling and cell migration [8, 9]. Patients with biallelic INPP5K variants present with bilateral cataracts, muscle weakness, and variable degree of intellectual disability [8, 9]. Similarities between MSS and the INPP5K-associated phenotype were observed not only at the clinical level but also on muscle pathology. Morphological examinations of muscle biopsies revealed the presence of vacuolated muscle fibres and at the ultrastructural level, electron-dense membranous structures surrounding degenerating myonuclei [2, 8]. Additionally, resemblance can be found at the molecular level: MSS is considered to be a disease of endoplasmic reticulum (ER) dysfunction, as loss of functional SIL1 [4] impacts on regular BiP functions including protein folding and ER-stress modulation [10]. Under basal conditions INPP5K localizes to the ER-membrane where it also interacts with BiP (via its C-terminus). Once formed at the ER-membrane, this functional BiP-INPP5K complex can be translocated to the plasma membrane in response to insulin stimulation [11]. Functional studies in patient fibroblasts revealed that *INPP5K* missense mutants are still competent enough to bind to BiP and do not affect the cellular response to stress, as abundances of well-known UPR markers seem to be mostly unchanged [8]. However, the relevance of the functional INPP5K-BiP interplay has not yet been fully elucidated.

In this study, we describe six new patients suffering from *INPP5K* mutations and hereby expand the mutational and clinical spectrum of the disease. Pathogenicity of two novel *INPP5K* missense mutations has been functionally confirmed. In addition, we systematically addressed the need to identify common molecular key players to further link MSS and the INPP5K-related phenotype as two rare diseases with considerable clinical overlaps. For this purpose, utilizing cells derived from patients with biallelic *INPP5K* and *SIL1* variants, we performed proteomic profiling and identified that PHGDH is significantly altered in abundance in the *in vitro* models of both diseases. Interestingly, autosomal recessive D-3-phosphoglycerate dehydrogenase or PHGDH mutations also result in a neurological phenotype clinically overlapping with MSS and INPP5K-related disease, and patients respond to L-serine treatment. Therefore we addressed the effect of L-serine treatment pre-clinically in generated zebrafish models of these genes. Thus, our study builds a molecular bridge between three rare neurological diseases with overlapping clinical features, and more importantly, allows translation from pre-clinical models to develop treatments for these rare neurological diseases.

MATERIALS AND METHODS

Cell culture

Skin biopsies were taken from three genetically proven (c.149T>C; p.Ile50Thr) *INPP5K* patients [8] as well as two genetically confirmed MSS patients (MSS2- 645+1G → A, skipping exon 6, homozygous and MSS4- 947_948insT, L316fs (het); 1030-18G → A, M344fs (het; [4]) and a total of five age-matched controls. Fibroblasts were grown in Dulbecco's modified Eagle's medium supplemented with 10% fetal bovine serum, 50 units/ml penicillin, 50 µg/ml streptomycin, 0.4% (v/v) amphotericin B (250 µg/ml), and 1 mm sodium pyruvate at 37 °C in a 5% CO_2 atmosphere. Fibroblasts were grown to 80% confluence prior to harvesting for proteomic profiling. Proteomic comparisons were carried out utilizing cells at similar passage numbers for each experiment. MSS patient-derived lymphoblastoid cells were generated and cultured as described before [12].

Measurement of WT and mutant INPP5K activity and structural model of INPP5K

Wild-type and mutant (p.Asp310Gly, p.Val23Ala, p.Leu55Phe) INPP5K were expressed in BL21 pLysS cells and purified on GSA beads (Thermo Fischer Scientific) in assay buffer (50 mM Tris-HCl, pH 7.5, 150 mM NaCl, 10 mM $MgCl_2$, 1% Triton X-100). The protein activity was then performed as previously described by Wiessner et al. [8].

The structural model of INPP5K mutants was determined by threading INPP5K sequence on the closest available orthologous crystal structures, OCRL (catalytic domain, PDB: 4CMN) and NDP52 (SKITCH domain, PDB: 3VVW), using the Phyre2 server [13].

Liquid chromatography coupled with mass spectrometry (LC-MS/MS) protein analysis

(See also supplemental document 1).

Data availability

INPP5K fibroblasts: The mass spectrometry proteomics data have been deposited to the ProteomeXchange Consortium via the PRIDE partner repository with the dataset identifier PXD009272. To visualize the data please use the username: reviewer26477@ebi.ac.uk and password: RdNNHLlo.

MSS fibroblasts: The mass spectrometry proteomics data have been deposited to the ProteomeXchange Consortium via the PRIDE partner repository with the dataset identifier PXD009297. To visualize the data please use the username: reviewer67767@ebi.ac.uk and password: eOUI5Dcd.

MSS lymphoblasts data set has PXD003030 as a identifier and can be found online via ProteomeXchange.

Zebrafish husbandry, morpholino knock-down and L-serine mediated phenotypic rescue

Zebrafish embryos and larvae were raised and staged according to standard procedures [14]. A Chameleon digital camera (model CMLN-13S2M, Chameleon) mounted to a Leica stereomicroscope was used to capture video recordings of embryos and light microscopy images were taken with a Leica dissection stereomicroscope equipped with a Leica digital camera (model DFC 420C).

A translation-blocking morpholino oligonucleotide (MO) targeting *phgdh* was designed and manufactured by Gene Tools (Pilomath, OR). Four previously published splice-blocking MOs were also used in our experiments. A *sil1* exon 2 splice-blocking MO [15] was purchased, as well as utilization of previously designed MO's directed against *inpp5ka* and *inpp5kb* [8]. The Gene Tools standard control MO targeting a human *β-haemoglobin* gene was used as a negative control for the effects of MO injections. MO sequence and injection concentrations are itemised in the supplementary table 1. Zygotes were injected following standard procedures [16]. Efficient gene knockdown was verified by western blot for *phgdh* translation-blocking MO and RT-PCR for splice blocking MOs [8, 15]. Knockdowns were performed in zygotes of the Golden (slc24a5b1/+) (ZIRC, OR, USA) and Tg (islet-1:GFP) [17] *Danio rerio* strains.

For attempted rescue of MO induced phenotypes in zebrafish models, E3 embryo medium (5mM NaCl, 0.17mM KCl, 0.33mM $CaCl_2$, 0.33mM MgSO4, 0.1% Methylene Blue) was supplemented with L-Serine (L-S) (Fisher Scientific) to final concentrations of 50, 75 and 100μM. At 24 hours post-fertilization (hpf) movements within the chorion of un-injected control and injected zebrafish – both treated and un-treated (L-S) – were observed and recorded (10x fish per variable, recorded for 2 minutes). Central nervous system neurons were imaged in treated and untreated Tg (islet-1:GFP) models.

Free L-serine analysis in zebrafish morphants:

We performed amino acid analysis in our zebrafish models (described above) to analyze the levels of free L-serine. Morphants were lysed using 1 % SDS lysis buffer (100 μL of 50 mM Tris-HCl (pH 7.8) buffer containing 150 mM NaCl, 1 % SDS, and Complete Mini using a manual glass grinder). After lysis ice cold ethanol (-20°C) was added to the samples at a ratio of 1:10. Samples were stored at -20°C overnight to allow the precipitation of macromolecules. Next, samples were centrifuged at 4°C and 18,000 g for 30 minutes which resulted in a precipitate that contains proteins and polypeptide chains while free amino acids were left in the ethanol solution which was evaporated using a SpeedVac.

Prior to analysis, the samples were further hydrolysed with 6 M HCL (Emprove Expert, SAFC, Merck) at 110°C for 22 h (gas-phase hydrolysis). Following this, residues were derivatized according to Cohen et al. [18]. Separation was done using reversed-phase high-performance liquid

chromatography. A 6-point calibration with amino acids standard solution (Amino acid Standard H, Thermo Fisher) was used to determine the amount of each detectable amino acid. The instable amino acids Tryptophan, Methionine and Cysteine were not taken into account.

Immunoblot analysis

Zebrafish and fibroblast protein extracts were separated by SDS-PAGE and transferred to Immobilon-FL PVDF membranes (Merck Millipore). Membranes were blocked for 1hr at room temperature with 5% milk in TBS-T and incubated with rabbit anti-PHGDH (Genetex; dilution 1:1000) overnight at 4°C. Blots were developed by incubation with horseradish peroxidase (HRP)-conjugated goat anti-mouse antibody (Invitrogen; dilution 1:5,000) overnight at 4˚C. Protein signals were detected with a SuperSignal™ West Femto Kit (Thermo Fisher Scientific) following the manufacturer's protocol.

IHC & Immunofluorescence Microscopy

Muscle Biopsies

Routine histological examinations (including H&E-, NADH-TR-, PAS- and SDH-staining) were carried out in addition to immunofluorescence-based studies of alpha-dystroglycan (Novus Biological 2238) and Merosin (Abcam ab140482) on the muscle biopsy specimen derived from index cases presented in our study. Moreover, muscle biopsy sections derived from three patients with homozygous c.149T>C p.Ile50Thr *INPP5K* mutations were analysed for abundance and distribution of INPP5K (SKIP C-19 Santa Cruz SC12073) and PHGDH (N-term antibody N1N2; GTX101948; Genetex) proteins. In addition, also on the muscle biopsies of patients with the homozygous *INPP5K* p.Ile50Thr mutation, H&E staining as well as fast and slow myosin fibre typing were carried out. The stainings were then visualized using an Axio Imager Z1 fluorescent microscope (Zeiss). Tiled images were obtained using a 10x objective and stitched together using the image processing facility provided in the Zen software package. The stitched images were then analysed using the open source image-processing package Fiji.

Zebrafish

Whole-mount immunofluorescence of zebrafish embryos was performed as previously described [19, 20]. Briefly, injected embryos were dechorionated with Pronase E (Sigma Aldrich) and euthanized by anaesthetic overdose. Embryos were then fixed in 4% paraformaldehyde/PBS overnight at 4°C, blocked at room temperature (RT) for 1 hr in 5% horse serum/PBS containing 0.1% Tween-20 and then incubated overnight at 4°C with primary antibody mouse anti-synaptic vesicle protein 2 (Developmental Studies Hybridoma Bank; dilution 1:200). Incubation with secondary antibody Alexa Fluor 488-conjugated goat anti-mouse IgG (Thermo Fisher; dilution 1:200) was performed for 1 hr at RT. Acetylcholine receptor clusters were stained with Alexa Fluor® 594 -conjugated α-bungarotoxin (Thermo Fisher; 1:1,000). Alexa Fluor® 594-conjugated phalloidin (Thermo Fisher; 1:100) was used to visualise actin filaments. Z-stack images of zebrafish were obtained by scanning one-half of the trunk myotome. Digital images were captured with a Nikon A1R laser scanning confocal microscope (Nikon, UK).

For the live examination of Isl1-GFP zebrafish, florescence embryos were anesthetized using 0.01% tricane and were mounted in 1.2 % agar on a depression slide glass as previously described (Westerfield et al., 1995) to avoid movement and drifts. Embryos were then visualized using a Zeiss florescence microscope with ApoTome attachment (Axio Imager Z1) using serial optical sections (Z-stacks) of approximatively 4 mm intervals. The image was then reconstructed from the stacked microscope images using Z project function (maximum intensity) from ImageJ.

Data availability

Data are available from the corresponding author upon reasonable request

RESULTS

1) Clinical and genetic findings in five novel patients with INPP5K-related disease expand the clinical and mutational spectrum of the phenotype

Patient 1 is a 25-year-old female (parents did not give consent for publication of photographs) born as the second child of non-consanguineous parents originating from a small town in southern Italy. The patient presented with cognitive delay since early infancy whereas motor milestones were

regularly achieved. By the age of 10 years, she started to present with progressive proximal muscle weakness. The first neuromuscular examination was performed at the age of 22 years and showed microcephaly and short stature (below the 3rd centile), severe hyperlordosis, pseudohypertrophy of calves and hypotrophy of quadriceps. Notably, the patient presented with an unsteady and waddling gait. Muscle weakness also involved proximal muscles of the upper limbs and the patient was unable to raise her arms above her shoulders (CK was elevated up to roughly 2 times of normal values). She also had a moderate intellectual disability. Brain MRI did not show cerebellar atrophy (Fig. 1). A biopsy of the quadriceps muscle showed dystrophic changes. Fibre diameter was variable with mildly increased perimysial connective tissue and centrally located myonuclei. Necrotic fibres were rarely detectable. Ophthalmological examination did not reveal the presence of cataracts [21].

Patient 2 is a 15-year-old boy (parents did not give consent for publication of photographs) also originating from a small town in southern Italy. The patient is the child of non-consanguineous parents. At 3 years of age, the boy underwent surgery for bilateral cataracts. He presented with mild cognitive and motor delay by early infancy and acquired autonomous ambulation at the age of 2 years. The first neurological examination of the patient was performed at age 4 years and revealed an ataxic gait and mild weakness of proximal muscles with positive Gower's sign. Remarkably, brain MRI of patient 2, performed at the age of 12 years, revealed mild cerebellar atrophy (Fig. 1). CK was elevated up to roughly 3 times the normal values. A muscle biopsy was performed at the age of 5 years and its examination revealed myopathic changes characterized by myofibre size variability, and internalized myonuclei. In the progression of the disease, the patient developed steppage gait indicative of distal muscles weakness and at the age of 14 he underwent orthopaedic surgery for clubfoot correction.

NGS revealed that both patient 1 and 2, harboured the previously described pathogenic homozygous nucleotide substitution c.67G>A (hg19: NM_016532.3), leading to the substitution of a non-polar aliphatic amino acid by a hydrophobic amino acid, p.Val23Met [9, 21].

Patients 3 & 4 are two sisters (Fig. 1) living in Reunion Island, born to a non-consanguineous couple of Creole descent. Both patients, aged 13 and 11 respectively, were investigated since early

childhood for muscle weakness associated with learning difficulties. Bilateral cataracts were observed in only one sister and required surgery at the age of 4 years. Investigation of serum CK levels revealed an elevation up to roughly 5 times of normal values. Patients also presented with mild (Patient 3) and moderate (Patient 4) intellectual disability. Brain MRIs did not reveal pathological changes (Fig. 1). Examination of the muscle biopsy specimens revealed a dystrophic pattern strongly suggesting a congenital muscular dystrophy (see below). Various genes were subsequently screened including *CAPN3* (a gene frequently involved muscular dystrophies in Reunion Island), *DMPK* (due to the association with cognitive deficits and early cataracts) and *FKRP* but did not show pathogenic sequence alterations. It is noteworthy that the mother developed early cataracts and underwent eye surgery at age 37.

The family was included within the "Myocapture project", a French project based on exome sequencing of patients and relatives to identify new genes responsible for neuromuscular diseases. The analysis was performed using the bioinformatics pipeline Polyweb and led to the identification of a new variant c.68T>C; p.(Val23Ala) in *INPP5K* (hg19: NM_016532.3), affecting the same amino acid, but resulting in a different change than in patients 1 and 2. Sanger sequencing confirmed the presence of the homozygous variant in the two affected girls and its segregation within the family members (heterozygous variant in the father and mother). Family relatedness scores have been calculated and the results showed no consanguinity in the parents both originating from La Reunion Island.

Patient 5 is now a 52-year-old female and was born after an uneventful pregnancy as the fourth child of non-consanguineous parents. Despite being able to walk independently at 14 months, she has had persistent walking difficulties throughout her childhood and has never being able to run. Myalgias and easy fatigability were also noticed in her infancy in addition to learning difficulties. She is also affected by high blood pressure and glaucoma. Height is 145 cm (<5°c) and occipital frontal circumference in the normal range for the height.

When first examined at age 42, the patient could only walk unsupported for short distances with a waddling gait. She was unable to get up from a chair without external support. Furthermore, the patient could neither squat nor raise her arms above her head. Neurological examination detected bilateral Babinski sign and a tendency to fall backwards on Romberg's manoeuvre. Mild bilateral

upper limb dysmetria with eyes closed were also noticed in addition to reduced but present tendon reflexes. Muscle strength on MRC scale showed weakness of the neck flexors = 3, neck extensors = 4, arm abductors = 4, hand finger extensors = 4, hip flexors = 2, hip extensors = 3, hip adductors and abductors = 3, knee flexors = 3, and ankle extensors = 4. The patient also reported intense muscle pain upon touch. No sensory deficits could be observed. CK was elevated up to 10-12 times of normal values. EMG/ENG revealed myopathic changes and a sensory axonal neuropathy. Moreover, somatosensory evoked potentials showed impairment of both peripheral and central somatosensory conduction. Brain MRI and spectroscopy as well as SPET revealed no significant abnormalities (data not shown). IQ was scored at 60 (mild mental retardation). Microscopic investigation revealed myopathic changes (see below). All the glycolytic enzyme activities were in the normal range. Remarkably, ophthalmological examination showed no overt cataracts. Investigation of pulmonary function revealed moderate restrictive impairment (FVC 72%) while heart ultrasound was normal [21].

In this patient, exome sequencing led to the identification of bi-allelic *INPP5K* mutations: compound heterozygosity was found for c.165G>T (hg19: NM_016532.3) resulting in a substitution of a non-polar hydrophobic by another non-polar hydrophobic amino acid (p.Leu55Phe) and c.753_756del (hg19: NM_016532.3) resulting in a frameshift (p.Arg251Serfs*24). *In silico*-based testing of pathogenicity of c.165G>T revealed a CADD score of 22.9 indicating that the variant is considered to be damaging. Mutations associated to the respective INPP5K-phenotypes are listed in table 1.

Patient 6 is a 10 year old girl, who was recently examined and diagnosed. Her parents are not consanguineous, but both of their families come from the Puglia region in Southern Italy. She was reported to be hypotonic at birth, her motor milestones were slightly delayed with the ability to freely walk at 18 months of age. She was diagnosed with bilateral cataracts, which were operated at age 3.5 years. In addition, short stature, a mild foot deformity and reduced mineral bone density were reported. She shows mild learning difficulties and receives special educational support. Neurological examination showed mild, proximal muscle weakness with a positive Gowers and difficulties to walk stairs. Brain MRI did not reveal any significant abnormalities.

Comparison of clinical findings obtained in patients 1-6 is provided in table 1 and shows that muscle vulnerability appears as a common clinical feature whereas cataracts is not always associated with causative variants in *INPP5K*. Moreover, additional clinical features such as mild cerebellar atrophy and sensory axonal neuropathy can be associated with the presence of *INPP5K* mutations expanding the currently known neurological spectrum of the disease. We hope that future description of *INPP5K* cases will aid will shed light to how often central nervous system pathologies occurs in this patients.

2) Testing of new *INPP5K* missense variants confirms pathogenicity and expands the pathomechanism of the disease

Given that INPP5K preferentially dephosphorylates PtdIns-4,5-P_2 at the D5 position [22] and previously described mutants show reduced catalytic activity [8], we performed *in vitro* measurements to assess the catalytic activity of the full-length p.Val23Ala as well as of p.Leu55Phe mutant INPP5K. Results show an impaired release of phosphate from PI(4,5)P_2 onto diC8 substrates for the p.Val23Ala mutant when compared with the full-length WT protein (Fig 2A). The artificial mutant pAsp310Gly (catalytic dead mutation) was included as a control. This reduced enzymatic activity might be explained by the fact that the p.Val23Ala mutation is localized in the 5-phosphatase domain of the protein (Fig 2B) and, as described for other mutants affecting the same region (including the previously reported p.Val23Met mutation identified in our patients 1 & 2), this leads to a destabilization of the overall shape of active site [8]. Studies of the catalytic activity of the p.Leu55Phe mutant form of INPP5K did not reveal a detrimental reduction in its activity against water soluble short-chain lipid substrate (Fig 2A), although this amino acid is also localized in the vicinity of the 5-phosphatase domain (Fig 2B). Extracting lipids, lipid immunostaining, and quantifying PI(4,5)P2 from patient material may help to determine, whether there is a difference in the total cellular levels of PI(4,5)P2 in the p.Leu55Phe-INPP5K mutant. However, there are currently no cellular models and the available muscle tissue is not sufficient to perform this analysis. Based on this finding we hypothesize that the amino acid substitution might trigger other pathophysiological mechanisms beyond its enzymatic activity, in association with the truncated p.Arg251Serfs*24 INPP5K present as compound heterozygous allele in patient 5.

3) Muscle biopsy findings in INPP5K patients are consistent with a congenital muscular dystrophy and do not reveal decrease of mutant INPP5K protein

H&E and Periodic acid-Schiff (PAS) reaction in a muscle biopsy specimen derived from patient 3 revealed a dystrophic pattern with occasionally centralized myonuclei (Fig 3A). The same dystrophic findings were observed in H&E-stained muscle sections derived from patient 5. Here, PAS staining further revealed increased reactivity in the sarcoplasm of a proportion of muscle fibres consistent with glycogen accumulation (Fig 3A). Several fibres with markedly increased SDH staining – suggestive for altered mitochondrial activity – could be observed in a proportion of muscle fibres (Fig 3A). A number of lobulated fibres presented with focal increase of NADH-TR reactivity (Fig 3A). For patients 1-4 abundance and distribution of alpha-dystroglycan and laminin-2 was studied by immunofluorescence and minor alterations were observed as exemplified for patients 1 and 2 (Fig. 3B).

To further investigate the INPP5K pathomechanism, muscle biopsy specimens derived from patients carrying the most common homozygous mutation, p.Ile50Thr [8] were investigated on the histological and immunological level. Results of H&E staining accord with a muscular dystrophy and fast/slow myosin staining did not indicate fibre-type grouping (Fig 3C). As missense mutations can influence structural and functional properties of proteins and consequently their stability, we explored the abundance/stability of mutant INPP5K protein by immunofluorescence studies in p.Ile50Thr-mutant INPP5K [8] and control muscle biopsies. We observed no reduced stability of p.Ile50Thr-mutant INPP5K (Fig 3D) according to our previous findings obtained in *in vitro* models over-expressing the wild type and mutant forms of INPP5K (8).

4) Proteomic studies of MSS- and INPP5K-mutant patient derived cells allow identification of PHGDH as a common molecular player

Given that clinical features of our five INPP5K-patients overlap with MSS features (Table 2), we aimed to identify biochemical key players linking MSS and the INPP5K-phenotype. We therefore performed proteomic profiling utilizing lymphoblastoid and fibroblast cells derived from MSS patients-caused by *SIL1* mutations- [4] as well as fibroblasts derived from INPP5K-patients [8]. Overall findings of our profiling utilizing MSS lymphoblastoid cells have already been described [12]. Proteomic analysis of MSS-patient derived fibroblasts allowed the quantification of 2996 proteins out of which 139 showed altered abundances and have been quantified based on at least two unique peptides. The proteomic response of INPP5K p.Ile50Thr-mutant fibroblasts revealed a statistically significant (p-Anova ≥ 0.05) altered abundance of 44 proteins (22 are increased and 22 are decreased) out of a total of 3018 identified proteins. Proteomics data have been deposited to the ProteomeXchange Consortium via the PRIDE [23] partner repository with the dataset identifiers PXD003030 (SIL1 lymphoblasts), PDX009297 (SIL1 fibroblasts), PXD009272 (INPP5K fibroblasts). After individual proteomic profiling, obtained data were filtered for proteins vulnerable in all three experiments. This approach allowed us to identify D-3-phosphoglycerate dehydrogenase (PHGDH) as a protein decreased in MSS patient derived cells but increased in p.Ile50ThrINPP5K mutated fibroblasts (Fig 4A). Immunoblot analysis of PHGDH levels in p.Ile50ThrINPP5K and control fibroblasts confirmed the increase in the patient derived cells (Fig 4A, right column). Quantitative analysis of PHGDH in cells is consistent with a statistically significant increase in Ile50Thr-INPP5K fibroblasts while in MSS fibroblasts, a decrease was observed (Suppl. fig 1). The focus on PHGDH was additionally prompted by the fact that recessive PHGDH mutations have already directly been linked to a neuropediatric phenotype with features common to MSS and INPP5K (Tab 2). To verify the proteomic results obtained in the patient-derived cells (p.Ile50Thr-INPP5K), we investigated the abundances and distribution of PHGDH in muscle biopsy specimens derived from patients harboring the p.Ile50Thr, p.Val23Met and p.Val23Ala-INPP5K variants [8]. Results of the immunofluorescence studies revealed an increase in PHGDH intensity in a proportion of muscle fibres in two out of the three p.Ile50Thr-INPP5K patients analyzed and in both of the p.Val23Met-INPP5K (Fig 4B and C). Overall quantification of fluorescence intensity confirmed a statistically significant (t-test < 0.05) PHGDH-increase in the INPP5K-patient derived biopsies compared to the two investigated control biopsies (Fig 4C). Unfortunately, biopsy material or fibroblasts from patients carrying the p.Leu55Phe and Arf251Serfs*24 mutations were not available.

Immunohistochemistry analysis of PHGDH in skeletal muscle derived from 26 weeks *woozy* mice (Fig 4E and F), the mouse model for MSS, shows a significant decrease (t-test ≤ 0.05) of PHGDH compared with the controls, thus supporting our data obtained from proteomics and immunofluorescence analysis of MSS fibroblasts.

The dysregulation of other proteins identified in our analysis (Figure 1 A) localized to the ER or other subcellular compartments such as the mitochondria might reflect the concomitant activation of further pro-survival or detrimental mechanisms. We might have to consider that these mechanisms can be tissue-specific.

5) SIL1, INPP5K and PHGDH zebrafish morphants show neurological phenotypes with overlapping pathology

To compare the phenotypical consequences of SIL1-, INPP5K- and PHGDH-depletion *in vivo,* respective zebrafish models (morphants) have been generated. The choice of zebrafish as animal models was prompted by the recent descriptions of INPP5K- and SIL1-morphants as suitable *in vivo* systems for the human phenotypes [8, 9, 15]. To the best of our knowledge, no zebrafish model for PHGDH has been previously described, therefore, we introduce here the first fish model for PHGDH deficiency (Fig 5A and B). A comparison of live embryo images of non-injected, control (CMO)- and *phgdh*-MO-injected zebrafish at 48 hpf revealed a spectrum of moderate to severe alterations of the tail at the light microscope level (Fig 5A). At 48hpf, the decreased expression of *phgdh* in injected zebrafish was confirmed via RT-PCR (data not shown) and given that PHGDH represents a common molecular denominator for MSS and INPP5K-CMD, as described above, PHGDH-protein levels were examined in the three different fish models by immunoblotting. As expected, no PHGDH-protein level could be detected in the *phgdh* morphants (Fig. 5C and D), whereas a slight increase of PHGDH in the *inpp5k* morphants and a decrease in the *sil1* morphants was detected. Additionally, PHGDH expression pattern is supported also by the amounts of free L-serine as *phgdh* and *sil1* morphants present with lower amounts compared to control embryos while *inpp5k a+b* zebrafish show an increase consistent with higher levels of PHGDH (Fig 5E). Our analysis was performed on whole embryos at 48 hpf. These results are in accordance with the proteomic findings obtained from the patient-derived cells (Fig. 4A).

Injection of the *phgdh*-MO led to an 8% increase in lethality of embryos compared to those injected with CMO (Fig 5F). Phalloidin-staining (labelling of actin cytoskeleton) was carried out to investigate skeletal muscle pathology and showed disruption of the regular chevron shape of somites, wavy fibres and, in some of the cases, absent notochord in the *phgdh*-MO fish compared to CMO injected zebrafish (Fig 5B). Moreover, NMJ-development is perturbed in the *phgdh*-MO injected embryos as seen by the reduced immunoreactivity of Synaptic vesicle glycoprotein 2 (SV2) suggesting a significant reduction of neuromuscular synapses in the dorsal region of the myotome segment, whereas the pre-patterning of the AChR clusters seems to be mostly unaffected (Fig 5B). Live imaging of the *phgdh*-MO injected transgenic Isl1:GFP zebrafish showed a strong effect of PHGDH-depletion on the development of the hindbrain visualized by a reduction of GFP-fluorescence intensity of the nerves Va, Vp, VI, VII and X (Fig 5B). Brain malformations have also been observed in the *Phgdh* deficient mouse model [24], thus confirming the suitability of this newly generated *phgdh* fish model.

The zebrafish model for MSS was recently introduced by Kawahara and colleagues [15]. The exact splice blocking morpholino targeting the splice acceptor site of exon 2 was employed for the generation of the *sil1* depleted zebrafish described in this study. A comparison of live embryo images of non-injected, control MO- and *sil1* MO-injected zebrafish at 48 hpf revealed a spectrum of mild to severe alterations of the tail already on the light microscopic level (Fig 5A). Embryos were injected with 6 ng of the morpholino, which reduced the expression of *sil1* compared to controls (data not shown). Injection of the *sil1*-MO led to a 11% increase in lethality of embryos compared to those injected with CMO (Fig 5G). Labelling of actin cytoskeleton via phalloidin in CMO and *sil1* fish at 48 hours post-fertilization displayed almost no abnormality of muscle fibre integrity. Although Kawahara and colleagues stated that at this morpholino concentration they are able to observe a disturbed muscle pattern and an affection of muscle fibre integrity [15], this finding could not be confirmed upon careful inspection in our experiment, which revealed only a very mild muscle phenotype (Fig. 5B). Perturbed NMJ-morphology in *sil1* MO-injected fish was recently described by our group [25] and could be recapitulated in this experiment: NMJs of *sil1* zebrafish show disruption of synapse formation along the myosepta, particularly at the presynaptic part of the NMJs (Fig 5B). This finding is in agreement with affected NMJs in both MSS patients and woozy mice (mouse model of MSS; [25]). Live imaging of the cranial motor neurons using the

transgenic Isl1:GFP fish showed an altered brain morphology with nerves III (oculomotor), IV (trochlear), VI (abduces) and VII (facial) being most vulnerable to the altered *sil1* expression (Fig 6B).

Morpholino-based depletion of *Inpp5ka* and *Inpp5kb* expression recapitulated the already described pathology in living embryos, including altered length and curvature of tails, difference of eye-to-head ratios [8, 9], muscle fibre defects and loss of the chevron shape of somites and deformation of myosepta (Fig 6B). The live imaging of *inpp5k a+b* morphant brains using Isl1:GFP transgenic zebrafish displayed mild abnormalities of the cranial nerves III, IV, VI and VII, exemplified by reduced fluorescence intensity (Fig 6B). As described previously, depletion of *inpp5ka+inpp5kb* does not alter NMJ-integrity in zebrafish (Fig 6B) [8].

6) L-serine treatment ameliorates the neuropathological phenotype in SIL1, INPP5K and PHGDH zebrafish morphants

Numerous publications have underlined the importance of L-serine (L-S; produced by PHGDH) in the development of the central nervous system (CNS) [26-28] and supplementation of L-S was found to have a beneficial effect on neurodegeneration in CNS disorders [29, 30]. Thus, rescue experiments were performed, in which L-S was supplemented in the growth media for the respective fish models, and the *phgdh* morphants included as proof-of-principle controls. Doing so, first the optimal dosage of L-S (ranging from 75 to 200μM) was determined using the non-injected and CMO-injected fish since previous reports of D-serine highlighted that a concentration of 1000 ppm has a detrimental effect on muscle and NMJ integrity [31]. Studies of skeletal muscle phenotype and survival rates (assessed at 48 hpf) revealed no differences between the 75 and 100 μM L-S. (Fig6 C). Given that *sil1*-MO (6 ng) injected embryos did not present a considerable muscle pathology, a possible improvement of myopathology upon L-S treatment would have been difficult to monitor. Thus, injection of 8 ng of the *sil1*-MO was carried out, resulting in a more pronounced muscle pathology and impact on the overall survival of the MSS-fish (Fig 5C).

3C). Treatment of the three different fish models (*sil1*-fish with 6 ng and 8 ng MO injection and 20 ng *phgdh* MO) with 100 μM L-S revealed that in *sil1*- and *phgdh*-morphants the mean survival ratio increased by 19% and 18%, respectively, when compared to the mock-treated group (Fig 6C).

In contrast, the survival rates remain mostly unchanged in the *inpp5k* treated and untreated morphants (Fig 6C).

To further verify the potential beneficial effects of L-S treatment, a comparative analysis of the morphology of treated and untreated fish was carried out: on the light microscopic level, *inpp5k*, *sil1*- and *phgdh*-MO injected fish treated with L-S for 48 hours presented no differences in comparison with the respective morpholino-injected fish models without treatment (Fig. 6A). However, further immunofluorescence-based morphological studies of vulnerable tissues revealed an amelioration of the slight decrease of fluorescence intensity of nerves VI and VII in *inpp5k* morphants upon L-S treatment (Fig 6B). Also, in the *sil1* morphants amelioration of decreased fluorescence intensity for cranial nerves the VI, VII and X (corresponding to abduces, facial and vagal nerves) could be detected upon L-S treatment (Fig 6B). In the *phgdh* morphants, upon L-S treatment, a marked improvement of the cranial nerves VI, VII and X in addition to Va and Vp as exemplified by an increase of the respective fluorescence-intensities, was observed (Fig 6B). Recovery of NMJ integrity upon L-S treatment was also assessed in the zebrafish models: immunofluorescence studies revealed a slight improvement of motor axon growth and synaptogenesis/axon extension along myosepta in treated *sil1*- and *phgdh*-MO injected embryos (Fig 6B) as shown by the Pearson's coefficient which expresses an increase in co-localization of the SV2 with the AChR (BT) (Suppl fig 2B). As expected, *inpp5k*-morphants present no changes in NMJ morphology (Fig 6B and Suppl fig 2B) upon L-S treatment. Investigation of the effect of L-S based intervention of the muscular phenotype in all three fish models revealed no effect in the *inpp5k*- morphants but did reveal a mild amelioration in the *sil1*- with a more positive effect on the myopathology in the *phgdh*-morphants (Fig. 6B).

We performed quantification of chorion movements [32] to monitor if L-S treatment could have a beneficial effect. Zebrafish embryos were recorded for 2 minutes and the normal tail movements (tail thrashes) were counted at 24 hpf. Non-injected zebrafish moved on average 4.7 times per minute and injection of the control MO reduced this to 4.1. No movements were recorded in the *inpp5ka+b* morphants, however the supplementation of L-S increased the movements to 2.4 per minute. The *sil1* morphants (8 ng of injected morpholino) treated with L-S presented with 4.1 movements per minute, a statistically significant increase (t-test < 0.05) compared with the mock treated *sil1* morphants, which showed 50% less movements (Fig 6D). The *phgdh*-morphant embryos *per se* presented with an irregular increase of tail movements catalogued as alternating

side tail thrash (18.6 movements/minute; Fig 6D) as a result of the severe neuronal phenotype. Despite the severe phenotype observed in this model, L-S treatment resulted in a statistically significant increase of tail trashes (41.2 movements/ minute; Fig 6D).

Prompted by our zebrafish results we have additionally assessed the cellular survival in three INPP5K [8] and two MSS [4] fibroblasts (Suppl fig 3) lines which showed up to 20 % increase in cellular viability in L-S MSS treated cells compared to non-treated ones while in INPP5K treated fibroblasts the viability increased just with 5% in line with the embryos viability we have obtained in our Fish models (Fig. 6C).

DISCUSSION

Genetic, clinical and muscle biopsy findings

Different pathogenic variants with a predominance of missense mutations in *INPP5K* have been recently associated with a syndromic form of congenital muscular dystrophy [8, 9, 21]. Applying whole exome sequencing in five patients, we identified two homozygous mutations affecting amino acid position 23 of *INPP5K* while the p.Val23Met missense mutation has already been described [9, 21], the p.Val23Ala mutation tested to be pathogenic by our further functional studies (Fig 2A&B) has not yet been reported. Additionally, a missense mutation affecting amino acid 55 (p.Leu55Phe) and a frameshift mutation affecting amino acid 251 (p.Arg251Serfs*24) – both also not reported so far in the literature –were identified. Hence, our clinical findings expand the current mutational spectrum of the disease, which is – based on the current literature – defined by the presence of congenital/early onset cataracts, mild intellectual disability and congenital myopathy. We now expand the INPP5K clinical phenotype that overlaps with MSS, as degeneration of the cerebellum represents a consistent finding in MSS patients as well as in woozy mice [6, 33, 34]. In the same context, absence of cataracts, as observed in one of our patients, has also been already described as an unusual finding in MSS [6]. With the presence of myalgias and an axonal neuropathy, our index patient 5 also contributes to the current spectrum of the INPP5K-phenotype. It is important to note that motor neuropathy has also been described in one MSS patient [35] and axonal vulnerability was recently shown in MSS, *sil1* morphant zebrafish and woozy mice [25].

A comprehensive study in patients with INPP5K variants reported on biochemical vulnerability of components of the dystrophin-associated glycoprotein complex (DGC), defining the phenotype as

a recessive form of congenital muscular dystrophy overlapping with MSS and dystroglycanopathy [9]. The histological findings in our patients cannot confirm the above described feature and rather support our previous findings, that proteins of the DGC are not necessarily affected by the INPP5K pathophysiology [8].

Consequently, the combined clinical findings in our patient cohort suggest that both rare neuropediatric diseases represent a clinical continuum, which might be caused by common pathophysiological cascades and mechanisms preventing the manifestation of clinical hallmarks in a minority of the patients.

Pathophysiological cascades and common treatment concept

A molecular link between MSS and the INPP5K-phenotype has already been suggested based on previous studies highlighting that both proteins bind to BiP and are involved in BiP-related processes controlling the ER organization and function [36]. While SIL1-loss results in perturbed protein processing associated with the massive build-up of protein aggregates [37, 38], these pathophysiological findings could not be identified in INPP5K-patient derived fibroblasts [8]. A possible explanation for this difference includes the localization and function of these proteins within the ER and distinct roles that result from the interaction of INPP5K, SIL1 with BiP respectively. While INPP5K is localized within the ER tubules (including distal portions) and is suggested to fine tune the ER organization [36], SIL1, is localized within the ER lumen and acts as a nucleotide exchange factor [39]. In skeletal muscle the interaction of INPP5K with BiP is necessary not only for its ER localization but also has been shown to regulate insulin signalling [36, 40], while the BiP-SIL1 interaction is necessary for protein production and folding [41]. Additionally, the presence of a residual INPP5K activity in patient muscle and fibroblasts can still modulate BiP related processes thus acting as a compensatory mechanism.

To obtain further insights into the molecular connection of MSS and INPP5K phenotypes, unbiased proteomic studies utilizing patient-derived cells were carried out and data intersection allowed the definition of PHGDH as a protein with decreased abundance in MSS patient-derived fibroblasts but increased abundance in INPP5K-patient derived fibroblasts (Fig 4). The decrease of PHGDH has recently been described by us in lymphoblastoid cells derived from MSS patients as well as in SIL1-vulnerable tissue derived from the woozy mouse model [12]. In addition, the same

study confirmed the increase of PHGDH upon the presence of ER-stress [12], supporting the idea that PHGDH expression is modulated by ER-stress [42].

PHGDH is a 3-phosphoglycerate dehydrogenase that catalyses the transformation of 3-phosphoglycerate to 3-hydroxyphosphopyruvate, which is the first step in the *de novo* biosynthesis of L-S from carbohydrates [43]. Patients suffering from recessive mutations in the *PHGDH* gene have either decreased levels of the corresponding protein or show a reduction of the catalytic activity of this enzyme resulting in decreased serine levels which in turn lead to phenotypical consequences such as intellectual disability, microcephaly and progressive neuropathy as well as occasionally encephalopathy with spasticity or seizures [44, 45]. Recurrent muscle contractions called infantile spasms are typical in this disorder, a primary muscle pathology has not been linked to PHGDH-deficiency. Most affected individuals have an infantile onset, which is the most severe form of the disease spectrum [45-47]. Recessive *PHGDH* mutations have been linked to the manifestation of another (neurological) syndromic phenotype characterized by microcephaly, cataracts, intellectual disability, mild cerebellar ataxia and axonal sensorimotor polyneuropathy [48]. Although of varying degrees of severity, these phenotypical findings show an overlap with the clinical presentation of the INPP5K-phenotype and MSS (Table 2). Consequently, our biochemical findings combined with the clinical manifestation of these diseases (also see above) lend further support to the hypothesis of a clinical continuum of rare neuropediatric diseases based on common pathophysiological cascades. Although primary involvement of skeletal muscle has not been explicitly described in PHDGH-patients, results of our zebrafish experiments reveal vulnerability of skeletal muscle upon reduction of PHGDH (Fig 5 and 6) expression *in vivo*. This observation is in agreement with the fact that PHGDH is crucial in muscle cell growth and has been recently found to be increased in skeletal muscle of patients with reversible myopathy [49, 50]. In our zebrafish models, PHGDH protein levels decreased in the *sil*-morpholino injected zebrafish (and in *phgdh*-morphants as a proof-of-principle) whereas the INPP5K-depletion correlated with a slight increase in PHGDH (Fig 5C and D). Free L-serine levels quantified in our zebrafish models are also in accordance with the expression of PHGDH in these morphants (Fig 5C-E). While the differences observed are relatively small, they may have biologically relevant effect. Free amino-acids represent approximatively 3 % of the total amino-acid pools and are potent activators of different signalling pathways at very low concentration [51].

Concordantly, our immunofluorescence studies, utilizing INPP5K-patient derived muscle biopsies, also revealed an increased abundance of PHGDH in a proportion of fibres (Fig 4B-D). L-S mediates neuroprotection also through the modulation of the ER-stress response [52]. Given that this cellular defence mechanism is perturbed in MSS pathophysiology (not in INPP5K) and that L-S treatment has already been successfully applied to ameliorate the PHGDH-phenotype in humans [48], we pre-clinically tested L-S treatment as a novel therapeutic strategy for INPP5K- and SIL1-related diseases in the respective zebrafish models. Overall L-S supplementation in zebrafish models demonstrated a hormetic effect of this amino-acid's concentration, which is a biphasic does response characterized by a beneficial effect at controlled does (75 and 100 µm) and an inhibitory or toxic effect at higher does, leading to embryonic lethality (over 200 µm). The small improvements seen in *inpp5k a+b* morphants might correlate with the observed increase of PHGDH in INPP5K-patients (and whole protein extracts from *inpp5k a+b* morphants) suggesting that an increase of L-S is already at a therapeutic level in these patients and acts as a cellular stress defence mechanism thus further elevation of this amino acid has no beneficial effect in terms of saturated compensation. Moreover, we observed that L-S treatment of MSS fibroblasts has a beneficial effect with an up to 20% increase in cellular survival, while INPP5K fibroblasts showed a minor increase only (5%) (Suppl. fig 3) This may support our hypothesis that further supplementation with L-S will in INPP5K disease models will not lead to major improvements as the levels of this amino acid are already at "therapeutic" levels through an endogenous compensatory mechanism.

Regarding the myopathic phenotypes, L-S treatment had no effect in the *inpp5k*-morphants, whereas in *sil1*-morphants and in *phgdh*-morphants a mild amelioration of muscle fibre disintegration could be detected (Fig 6B). Given this, one might assume that in SIL1-myopathy, PHGDH reduction is a stronger general contributor to the overall muscle pathophysiology than in INPP5K-myopathy, where, in contrast, the levels of this protein are elevated.

Cranial nerves in all *sil1* and *phgdh* fish models greatly benefit from the increased concentration of L-S while the *inpp5k a+b* morphants show minor changes (Fig 6B). Numerous publications have underlined the importance of L-S in CNS development, as supplementation of L-S was found to have a beneficial effect on neurodegeneration in CNS disorders [29, 53]. L-S was shown to be an astroglia-derived trophic factor for Purkinje neurons [46], a population highly affected by the loss of SIL1 [34, 46]. Here we show that the same cellular population might also be affected in INPP5K

patients as mild cerebellar atrophy was shown in one patient. We hypothesise based on our data that an elevation of PHGDH in INPP5K patients contribute to the morphological rescue of the brain and that lower levels of this enzyme might contribute to a neurological phenotype as seen in Patient 2 (Table 1).

Combined results of our pre-clinical interventional study suggest that MSS and INPP5K patients might benefit from L-S intake whereby a greater effect on the nervous system phenotype than on the muscle phenotype can be predicted. L-S has been used successfully without any major side effects in patients with Amyotrophic Lateral Sclerosis which have received approximatively twice a day 15 grams of L-S [29]. Recent studies have demonstrated that L-S administration might be also beneficial for patients with Alzheimer's [30]. It is important to note here that the FDA states L-S is generally regarded as safe as long as it consists of no more than 8.4% of total protein in the diet [29].

Conclusions:

Within this study, the description of six new patients suffering from *INPP5K* mutations expanded both the mutational and phenotypical spectrum of the underlying disease. The latter aspect is of particular importance for clinical evaluation and suggestion of candidate genes. Results of our proteomic profiling experiments allowed the definition of a first "molecular puzzle" of three rare neuromuscular diseases with striking phenotypical (syndromic) overlap (Table 2) via altered abundance of PHGDH. A therapeutic potential of this new acquired knowledge has been directly implicated by treatment of our zebrafish models phenocopying the human diseases with L-serine and thus suggests that this approach might be beneficial for MSS and INPP5K patients respectively.

Acknowledgements:

We thank Mrs. Nancy Meyer for her technical expert assistance. Prof. Dr. Jan Senderek (Friedrich-Baur Institute Munich, Germany) kindly provided the cells derived from MSS-patients.

Funding:

This work was supported by a grant from the Deutsche Forschungsgemeinschaft (to R. Z.; ZA 639/1-1), by the Deutsche Gesellschaft für Muskelkranke (to A.R.). Moreover, financial support by the French Muscular Dystrophy Association (AFM-Téléthon; grant 21466 to A.R., grant 22429 to L.S. and postdoctoral fellowship to EOC), the Ministerium für Kultur und Wissenschaft des Landes Nordrhein-Westfalen, the Der Regierende Bürgermeister von Berlin, Senatskanzlei Wissenschaft und Forschung is gratefully acknowledged. The Institut National de la Santé et de la Recherche Médicale, the Sorbonne Université- Faculté de Médecine, the Association Française contre les Myopathies and France Génomique (Myocapture Project), National Research Agency, Investment for the Future (Grant No. ANR-10-INBS-09) also supported this work. HL receives support from the Canadian Institutes of Health Research (Foundation Grant FDN-167281), the Canadian Institutes of Health Research and Muscular Dystrophy Canada (Network Catalyst Grant for NMD4C), the Canada Foundation for Innovation (CFI-JELF 38412), and the Canada Research Chairs program (Canada Research Chair in Neuromuscular Genomics and Health, 950-232279). RH was supported by the European Research Council [309548], the Wellcome Investigator Award [109915/Z/15/Z]. the Medical Research Council (UK) [MR/N025431/1]; the Wellcome Trust Pathfinder Scheme [201064/Z/16/Z], the Newton Fund [UK/Turkey, MR/N027302/1], the Lily Foundation and the Evelyn Trust.

Competing interest:

The authors report no competing interests.

Figure legends:

Figure 1: Clinical and brain imaging findings in novel INPP5K-patients. (**A**) representative photographs of patient 3 and 4 showing severe hyperlordosis. (**B**) Brain MRI of patients 1-4 showing no brain abnormalities in patients 1, 3 and 4 but a mild cerebellar atrophy in patient 2. Size of oculomotor muscles appears normal in patients 3 & 4 and lenses have obviously been removed with vacuity of the eyes in patient 3 whereas in patient 4 the lenses have not been removed and are well visible within the eye-balls. 1-lateral view; 2-overhead view; 3and 4-ocular view.

Figure 2. Enzymatic activity of novel missense mutation in INPP5K. (A) Quantification of enzymatic activity of novel missense mutants of INPP5K. GST-INPP5K was bacterially expressed and purified and exposed to the water soluble substrate $PI(4,5)P_2$ diC_8, Phosphate released by hydrolysis of $PI(4,5)P_2$ was measured by malachite assay, and the engineered catalytic null mutant $INPP5K^{Asp310Gly}$ was included as a negative control. GST-$INPP5K^{Val23Met}$ has significantly compromised enzymatic activity in this assay (n=3 per condition, t-test), whereas GST-INPP5KLeu55Phe retains near- wildtype levels of activity against water soluble substrate (n=4 wells per condition, t-test). **(B)** Predicted structure of the INPP5K catalytic domain, modelled using Phyre2 [13]. Val23 (yellow) is in the catalytic pocket of the enzyme (red), whereas Leu55 is an internal residue close to a predicted hydrophobic finger (hydrophobic residues coloured blue), which in the enzyme OCRL is thought to assist in associating the catalytic domain with highly curved membranes.

Figure 3: Muscle biopsy findings in INPP5K-patients. (**A**) Representative histological findings in two (patient 3 & 5) of the five novel INPP5K patients include variation in fiber size, rounding of fibers, increased endomysial collagen and some degree of fatty degeneration as well as focal increase of glycogen as measured by periodic acid-Schiff (PAS) staining in some fibers (black arrows) and focal increase of mitochondria in a proportion of fibers as measured by nicotinamidadenindinucleotide tetrazolium reductase (NADH-TR) reaction (black arrows). Moreover, high oxidative activity is indicated in a proportion of fibers by succinic dehydrogenase (SDH) reaction. (**B**) Immunofluorescence-based analyses of alpha-dystroglycan and merosin (shown for patients 1 & 2) did not show changes which would accord with a vulnerability of both proteins upon the loss of functional INPP5K. (**C**) Findings in two INPP5K-patients with p.Ile50Thr

mutation [8]; H&E stain (left panel) revealing variation in fiber size, rounding of fibers, increased endomysial collagen and some degree of fatty degeneration. Immunohistochemical analysis focusing on fast (middle panel) and slow (right panel) myosin revealed a predominance of fast fibres in patient 6 compared with patient 7. Atrophy of slow fibres some of which were grouped was variably seen in both patients together with co-expression of both myosin isoforms. (**D**) Immunofluorescence-based analysis of INPP5K expression/ stability did not reveal changes in abundance or distribution between control and patients 6 & 7 (p.Ile50Thr mutation).

Figure 4: Workflow depicting our protein studies on fibroblasts derived from MSS- and INPP5K-patients. **(A)** For MSS-patients, immortalized lymphoblastoid cells and primary fibroblasts have been used for iTRAQ-labelling and subsequent peptide-fractionation followed by LC-MS/MS analyses (left and middle column). For primary fibroblast cells derived from INPP5K-patients (all with p.Ile50Thr mutation), label-free protemic profiling was carried out (right column). In all three experiments, as shown by the precursor and reporter ion intensities of the respective experiments (exemplified by the unique peptides of PHGDH i.e. GTIQVITQGTSLK in label-free and QADVNLVNAK in labelling approaches, respectively), PHGDH was altered in abundance: in SIL1-patient derived cells, a statistically significant decrease could be detected whereas in INPP5K-patient derived fibroblasts, a statistically significant increase could be identified. This increase in INPP5K fibroblasts was also confirmed by immunoblotting. The volcano plots highlight our overall proteomic findings: each red and green dot represents a protein altered with a p-Anova ≥ 0.05. (**B**) Representative PHGDH-staining in a muscle biopsy specimen of a control subject (upper panel) and of a INPP5K-patient harbouring the p.Ile50Thr and p.Val23Met mutation (lower panel) showing an increase of PHGDH in a proportion of diseased muscle fibres. Scale bars: 200μm. (**C** and **D**) Box plot depicting the florescence data points measured in two controls and three (p.Ile50Thr) respectively two (p.Val23Met and p.Val23Ala) patients. The central band represents the median, the lower and upper hinges correspond to the first and third quartiles (25 and 75%) while the whiskers extend to the highest and lowest points within the data (1.5× the inter-quartile range). Results were observed in one (n=1) independent experiments (due to the limited amount of sample). Statistical analysis unpaired Student's *t*-test was employed where $*P \leq 0.05$ was considered statistically significant. (**E**) Immunohistochemistry analysis of PHGDH on paraffin sections from paraformaldehyde-fixed

quadriceps muscle specimens of 26-week-old wild type and three *woozy* mouse muscle. Scale bars: 22 μm (**F**) Optical Density (OD) determination of (F) where graph show the results of our three independent experiments resulted from the analysis of three controls and three woozy mice. Data represent mean ± SEM, statistical analysis unpaired Student's *t*-test was employed where $*P \leq 0.05$ was considered statistically significant. Similar results were observed in at least three (n=3) independent experiments.

Figure 5: Phenotyping of *phgdh*- and *sil1*-morphants. (**A**) Morpholino-based depletion of *phgdh* and *sil1* in 48 hpf zebrafish resulted in abnormal curvature of the tails of both models compared to wildtype (WT) and control-morpholino (CMO) injected ones. (**B**) Immunofluorescence-based studies of tissue morphologies revealed disintegration of muscle fibres visualized by phalloidin staining (first lane), abnormal patterning of the pre-synaptic NMJs visualized by reduced SV2-immunoreactivity (lanes 2-4) and abnormal development of the brain affecting the cranial nerves (lane 5) in both fish models. Scale bars: 50 μm. Regarding brain abnormalities, in *phgdh*-morphants nerves Va, Vp, VI, VII, X and in *sil1*-morphants nerves III, IV, VI, VII and X are vulnerable to the loss of the respective protein expression. Scale bars: 100 μm. Similar results were observed in at least four (n=4) independent experiments. (**C**) Western Blot- studies of PHGDH protein level in the three fish models revealed a slight increase in whole protein extracts of *inpp5k*-morphants but a considerable decrease in the *sil1*-morphants as well as in the *phgdh*-morphants. (**D**) Decrease of the PHGDH protein in the *phgdh*-morphants reflects the successful morpholino-based depletion of the expression of the corresponding gene as also depicted quantitatively. Data represent mean ± SEM, statistical analysis unpaired Student's *t*-test was employed where $*P \leq 0.05$ was considered statistically significant. Similar results were observed in at least three (n=3) independent results. (**E**) Free L-serine analysis in whole embryos at 48 hpf by liquid chromatography. Results accord with the PHGDH expression in zebrafish. Data represent mean ± SEM, statistical analysis unpaired Student's *t*-test was employed where $*P \leq 0.05$ was considered statistically significant. Similar results were observed in at least two (n=2) independent experiments due to the high amount of embryos needed for this analysis. (**F** and **G**) Depletion of *phgdh* and *sil2* is also associated with reduced survival of the fish at 48 hpf. The central band represents the median, the lower and upper hinges correspond to the first and third

quartiles (25 and 75%) while the whiskers extend to the highest and lowest points within the data (1.5× the inter-quartile range). Statistical analysis unpaired Student's *t*-test was employed where $*P \leq 0.05$ was considered statistically significant. Similar results were observed in at least four (n=4) independent experiments.

Figure 6: L-serine treatment studies in *phgdh*-, *sil1*- and *inpp5k*-morphants: (**A**) Study of the effect of L-S treatment (100 μM) on the phenotype of the fish did not reveal changes on the curvature of the tail in the *inpp5k*- and *sil1*-morphants, whereas a slight beneficial effect could be observed in the *phgdh*-morphants, 30 fish were analyzed per condition. Scale bars: 500 μm (**B**) Results of immunofluorescence-based studies of L-S treatment (100 μM) in tissues vulnerable against the depletion of *inpp5k*-, *sil1*- and *phgdh*-expression. A slight amelioration of muscle fibre integrity can only be identified in the *phgdh*-morphants but not in the two other models. A minimum of 10 fish were analyzed per condition. Scale bars: 50 μm. In contrast, the pre-synaptic phenotype was ameliorated in the *sil1*- as well as in the *phgdh*-morphants, as exemplified by an increase of SV2-immunoreactivity (*inpp5k*-morphants did not show an NMJ-phenotype *per se*). A minimum of 10 fish were analyzed per condition. Scale bars: 50 μm. In addition, GFP-fluorescence intensity suggests that the cranial nerves III, IV, VI and VII improved in *inpp5k*-morphants. *sil1*-morphants showed a phenotype amelioration of the nerves VI, VII as well as X and the *phgdh*-morphants of nerves Va, Vp, VI, VII and X after treatment based on increased GFP-fluorescence intensity. A minimum of 10 fish were analyzed per condition. Scale bars: 100 μm. (**C**) Survival rates of zebrafish disease models treated with 75 and 100 μM of L-serine, respectively. Whereas L-serine treatment has no impact on survival of wildtype fish, an effect on morphant-survival can be observed for the three different disease models Data represent mean ± SEM, statistical analysis unpaired Student's *t*-test was employed where $*P \leq 0.05$ was considered statistically significant (**D**) L-S treatment did not show an effect on the number of tail thrashes per minute in the WT and CMO fish but a statistically significant increase in *sil1*-, *inpp5k*- and *phgdh*-morphants, n=12 fish from 3 different experiments were investigated per condition. The central band represents the median, the lower and upper hinges correspond to the first and third quartiles (25 and 75%) while the whiskers extend to the highest and lowest points within the data (1.5× the inter-quartile range). Statistical analysis unpaired Student's *t*-test was employed where $*P \leq 0.05$ was considered

statistically significant. Similar results were observed in at least three (n=3) independent experiments.

References:

1. Marinesco G, Draganesco S, D V. Nouvelle maladie familiale caractérisée par une cataracte congénitale et un arrêt du développement somato-neuro-psychique. *Encephale*. 1931;26:97-109.

2. Sewry CA, Voit T, Dubowitz V. Myopathy with unique ultrastructural feature in Marinesco-Sjogren syndrome. *Annals of neurology*. Oct 1988;24(4):576-80. doi:10.1002/ana.410240416

3. Sjogren T. Hereditary congenital spinocerebellar ataxia accompanied by congenital cataract and oligophrenia; a genetic and clinical investigation. *Confinia neurologica*. 1950;10(5):293-308.

4. Senderek J, Krieger M, Stendel C, et al. Mutations in SIL1 cause Marinesco-Sjogren syndrome, a cerebellar ataxia with cataract and myopathy. *Nature genetics*. Dec 2005;37(12):1312-4. doi:10.1038/ng1678

5. Anttonen AK, Mahjneh I, Hamalainen RH, et al. The gene disrupted in Marinesco-Sjogren syndrome encodes SIL1, an HSPA5 cochaperone. *Nature genetics*. Dec 2005;37(12):1309-11. doi:10.1038/ng1677

6. Krieger M, Roos A, Stendel C, et al. SIL1 mutations and clinical spectrum in patients with Marinesco-Sjogren syndrome. *Brain : a journal of neurology*. Dec 2013;136(Pt 12):3634-44. doi:10.1093/brain/awt283

7. Munro S, Pelham HR. An Hsp70-like protein in the ER: identity with the 78 kd glucose-regulated protein and immunoglobulin heavy chain binding protein. *Cell*. Jul 18 1986;46(2):291-300.

8. Wiessner M, Roos A, Munn CJ, et al. Mutations in INPP5K, Encoding a Phosphoinositide 5-Phosphatase, Cause Congenital Muscular Dystrophy with Cataracts and Mild Cognitive Impairment. *American journal of human genetics*. Mar 02 2017;100(3):523-536. doi:10.1016/j.ajhg.2017.01.024

9. Osborn DP, Pond HL, Mazaheri N, et al. Mutations in INPP5K Cause a Form of Congenital Muscular Dystrophy Overlapping Marinesco-Sjogren Syndrome and Dystroglycanopathy.

American journal of human genetics. Mar 02 2017;100(3):537-545. doi:10.1016/j.ajhg.2017.01.019

10. Hendershot LM. The ER function BiP is a master regulator of ER function. *The Mount Sinai journal of medicine, New York*. Oct 2004;71(5):289-97.

11. Ijuin T, Hatano N, Takenawa T. Glucose-regulated protein 78 (GRP78) binds directly to PIP3 phosphatase SKIP and determines its localization. *Genes to cells : devoted to molecular & cellular mechanisms*. May 2016;21(5):457-65. doi:10.1111/gtc.12353

12. Kollipara L, Buchkremer S, Coraspe JAG, et al. In-depth phenotyping of lymphoblastoid cells suggests selective cellular vulnerability in Marinesco-Sjogren syndrome. *Oncotarget*. Sep 15 2017;8(40):68493-68516. doi:10.18632/oncotarget.19663

13. Kelley LA, Mezulis S, Yates CM, Wass MN, Sternberg MJ. The Phyre2 web portal for protein modeling, prediction and analysis. *Nat Protoc*. Jun 2015;10(6):845-58. doi:10.1038/nprot.2015.053

14. Kimmel CB, Ballard WW, Kimmel SR, Ullmann B, Schilling TF. Stages of embryonic development of the zebrafish. *Dev Dyn*. Jul 1995;203(3):253-310. doi:10.1002/aja.1002030302

15. Kawahara G, Hayashi YK. Characterization of Zebrafish Models of Marinesco-Sjogren Syndrome. *PLoS One*. 2016;11(10):e0165563. doi:10.1371/journal.pone.0165563

16. Rosen JN, Sweeney MF, Mably JD. Microinjection of zebrafish embryos to analyze gene function. *J Vis Exp*. Mar 9 2009;(25)doi:10.3791/1115

17. Higashijima S, Hotta Y, Okamoto H. Visualization of cranial motor neurons in live transgenic zebrafish expressing green fluorescent protein under the control of the islet-1 promoter/enhancer. *J Neurosci*. Jan 1 2000;20(1):206-18.

18. Cohen SA, Michaud DP. Synthesis of a fluorescent derivatizing reagent, 6-aminoquinolyl-N-hydroxysuccinimidyl carbamate, and its application for the analysis of hydrolysate amino acids via high-performance liquid chromatography. *Anal Biochem*. Jun 1993;211(2):279-87. doi:10.1006/abio.1993.1270

19. Muller JS, Jepson CD, Laval SH, Bushby K, Straub V, Lochmuller H. Dok-7 promotes slow muscle integrity as well as neuromuscular junction formation in a zebrafish model of

congenital myasthenic syndromes. *Hum Mol Genet*. May 1 2010;19(9):1726-40. doi:10.1093/hmg/ddq049

20. Senderek J, Muller JS, Dusl M, et al. Hexosamine biosynthetic pathway mutations cause neuromuscular transmission defect. *American journal of human genetics*. Feb 11 2011;88(2):162-72. doi:10.1016/j.ajhg.2011.01.008

21. D'Amico A, Fattori F, Nicita F, et al. A Recurrent Pathogenic Variant of INPP5K Underlies Autosomal Recessive Congenital Muscular Dystrophy With Cataracts and Intellectual Disability: Evidence for a Founder Effect in Southern Italy. *Front Genet*. 2020;11:565868. doi:10.3389/fgene.2020.565868

22. Schmid AC, Wise HM, Mitchell CA, Nussbaum R, Woscholski R. Type II phosphoinositide 5-phosphatases have unique sensitivities towards fatty acid composition and head group phosphorylation. *FEBS letters*. Oct 08 2004;576(1-2):9-13. doi:10.1016/j.febslet.2004.08.052

23. Deutsch EW, Csordas A, Sun Z, et al. The ProteomeXchange consortium in 2017: supporting the cultural change in proteomics public data deposition. *Nucleic Acids Res*. Jan 4 2017;45(D1):D1100-D1106. doi:10.1093/nar/gkw936

24. Yang JH, Wada A, Yoshida K, et al. Brain-specific Phgdh deletion reveals a pivotal role for L-serine biosynthesis in controlling the level of D-serine, an N-methyl-D-aspartate receptor co-agonist, in adult brain. *J Biol Chem*. Dec 31 2010;285(53):41380-90. doi:10.1074/jbc.M110.187443

25. Phan V, Cox D, Cipriani S, et al. SIL1 deficiency causes degenerative changes of peripheral nerves and neuromuscular junctions in fish, mice and human. *Neurobiol Dis*. Apr 2019;124:218-229. doi:10.1016/j.nbd.2018.11.019

26. Yoshida K, Furuya S, Osuka S, et al. Targeted disruption of the mouse 3-phosphoglycerate dehydrogenase gene causes severe neurodevelopmental defects and results in embryonic lethality. *J Biol Chem*. Jan 30 2004;279(5):3573-7. doi:10.1074/jbc.C300507200

27. de Koning TJ, Snell K, Duran M, Berger R, Poll-The BT, Surtees R. L-serine in disease and development. *Biochem J*. May 1 2003;371(Pt 3):653-61. doi:10.1042/BJ20021785

28. Tabatabaie L, Klomp LW, Berger R, de Koning TJ. L-serine synthesis in the central nervous system: a review on serine deficiency disorders. *Mol Genet Metab*. Mar 2010;99(3):256-62. doi:10.1016/j.ymgme.2009.10.012

29. Levine TD, Miller RG, Bradley WG, et al. Phase I clinical trial of safety of L-serine for ALS patients. *Amyotroph Lateral Scler Frontotemporal Degener*. Feb 2017;18(1-2):107-111. doi:10.1080/21678421.2016.1221971

30. Le Douce J, Maugard M, Veran J, et al. Impairment of Glycolysis-Derived l-Serine Production in Astrocytes Contributes to Cognitive Deficits in Alzheimer's Disease. *Cell Metab*. Mar 3 2020;31(3):503-517 e8. doi:10.1016/j.cmet.2020.02.004

31. Chen XG, Wang YH, Wen CC, Chen YH. Overdose of D-serine Induces Movement Disorder and Neuromuscular Changes of Zebrafish Larvae. *J Toxicol Pathol*. Apr 2014;27(1):19-24. doi:10.1293/tox.2013-0032

32. Menelaou E, Husbands EE, Pollet RG, Coutts CA, Ali DW, Svoboda KR. Embryonic motor activity and implications for regulating motoneuron axonal pathfinding in zebrafish. *Eur J Neurosci*. Sep 2008;28(6):1080-96. doi:10.1111/j.1460-9568.2008.06418.x

33. Zhao L, Longo-Guess C, Harris BS, Lee JW, Ackerman SL. Protein accumulation and neurodegeneration in the woozy mutant mouse is caused by disruption of SIL1, a cochaperone of BiP. *Nature genetics*. Sep 2005;37(9):974-9. doi:10.1038/ng1620

34. Buchkremer S, Gonzalez Coraspe JA, Weis J, Roos A. Sil1-Mutant Mice Elucidate Chaperone Function in Neurological Disorders. *J Neuromuscul Dis*. May 27 2016;3(2):169-181. doi:10.3233/JND-160152

35. Byrne S, Dlamini N, Lumsden D, et al. SIL1-related Marinesco-Sjoegren syndrome (MSS) with associated motor neuronopathy and bradykinetic movement disorder. *Neuromuscul Disord*. Jul 2015;25(7):585-8. doi:10.1016/j.nmd.2015.04.003

36. Dong R, Zhu T, Benedetti L, et al. The inositol 5-phosphatase INPP5K participates in the fine control of ER organization. *J Cell Biol*. Oct 1 2018;217(10):3577-3592. doi:10.1083/jcb.201802125

37. Roos A, Buchkremer S, Kollipara L, et al. Myopathy in Marinesco-Sjogren syndrome links endoplasmic reticulum chaperone dysfunction to nuclear envelope pathology. *Acta neuropathologica*. May 2014;127(5):761-77. doi:10.1007/s00401-013-1224-4

38. Roos A, Kollipara L, Buchkremer S, et al. Cellular Signature of SIL1 Depletion: Disease Pathogenesis due to Alterations in Protein Composition Beyond the ER Machinery. *Mol Neurobiol*. Oct 2016;53(8):5527-41. doi:10.1007/s12035-015-9456-z

39. Dudek J, Benedix J, Cappel S, et al. Functions and pathologies of BiP and its interaction partners. *Cell Mol Life Sci*. May 2009;66(9):1556-69. doi:10.1007/s00018-009-8745-y

40. Ijuin T, Hatano N, Hosooka T, Takenawa T. Regulation of insulin signaling in skeletal muscle by PIP3 phosphatase, SKIP, and endoplasmic reticulum molecular chaperone glucose-regulated protein 78. *Biochim Biophys Acta*. Dec 2015;1853(12):3192-201. doi:10.1016/j.bbamcr.2015.09.009

41. Ichhaporia VP, Kim J, Kavdia K, et al. SIL1, the endoplasmic-reticulum-localized BiP co-chaperone, plays a crucial role in maintaining skeletal muscle proteostasis and physiology. *Dis Model Mech*. May 10 2018;11(5)doi:10.1242/dmm.033043

42. Dombroski BA, Nayak RR, Ewens KG, Ankener W, Cheung VG, Spielman RS. Gene expression and genetic variation in response to endoplasmic reticulum stress in human cells. *American journal of human genetics*. May 14 2010;86(5):719-29. doi:10.1016/j.ajhg.2010.03.017

43. Pacold ME, Brimacombe KR, Chan SH, et al. Corrigendum: A PHGDH inhibitor reveals coordination of serine synthesis and one-carbon unit fate. *Nature chemical biology*. Jul 19 2016;12(8):656. doi:10.1038/nchembio0816-656

44. Tabatabaie L, Klomp LW, Rubio-Gozalbo ME, et al. Expanding the clinical spectrum of 3-phosphoglycerate dehydrogenase deficiency. *J Inherit Metab Dis*. Feb 2011;34(1):181-4. doi:10.1007/s10545-010-9249-5

45. van der Crabben SN, Verhoeven-Duif NM, Brilstra EH, et al. An update on serine deficiency disorders. *J Inherit Metab Dis*. Jul 2013;36(4):613-9. doi:10.1007/s10545-013-9592-4

46. Furuya S, Tabata T, Mitoma J, et al. L-serine and glycine serve as major astroglia-derived trophic factors for cerebellar Purkinje neurons. *Proceedings of the National Academy of Sciences of the United States of America*. Oct 10 2000;97(21):11528-33. doi:10.1073/pnas.200364497

47. Pind S, Slominski E, Mauthe J, et al. V490M, a common mutation in 3-phosphoglycerate dehydrogenase deficiency, causes enzyme deficiency by decreasing the yield of mature enzyme. *J Biol Chem*. Mar 01 2002;277(9):7136-43. doi:10.1074/jbc.M111419200

48. Brassier A, Valayannopoulos V, Bahi-Buisson N, et al. Two new cases of serine deficiency disorders treated with l-serine. *Eur J Paediatr Neurol*. Jan 2016;20(1):53-60. doi:10.1016/j.ejpn.2015.10.007

49. Brown DM, Williams H, Ryan KJ, et al. Mitochondrial phosphoenolpyruvate carboxykinase (PEPCK-M) and serine biosynthetic pathway genes are co-ordinately increased during anabolic agent-induced skeletal muscle growth. *Sci Rep*. Jun 28 2016;6:28693. doi:10.1038/srep28693

50. Hathazi D, Griffin H, Jennings MJ, et al. Metabolic shift underlies recovery in reversible infantile respiratory chain deficiency. *EMBO J*. Dec 1 2020;39(23):e105364. doi:10.15252/embj.2020105364

51. Falco F, Barra M, Cammarata M, et al. Amino acid composition in eyes from zebrafish (Danio rerio) and sardine (Sardina pilchardus) at the larval stage. *Springerplus*. 2016;5:519. doi:10.1186/s40064-016-2137-1

52. Dunlop RA, Powell JT, Metcalf JS, Guillemin GJ, Cox PA. L-Serine-Mediated Neuroprotection Includes the Upregulation of the ER Stress Chaperone Protein Disulfide Isomerase (PDI). *Neurotox Res*. Jan 2018;33(1):113-122. doi:10.1007/s12640-017-9817-7

53. Garofalo K, Penno A, Schmidt BP, et al. Oral L-serine supplementation reduces production of neurotoxic deoxysphingolipids in mice and humans with hereditary sensory autonomic neuropathy type 1. *J Clin Invest*. Dec 2011;121(12):4735-45. doi:10.1172/JCI57549

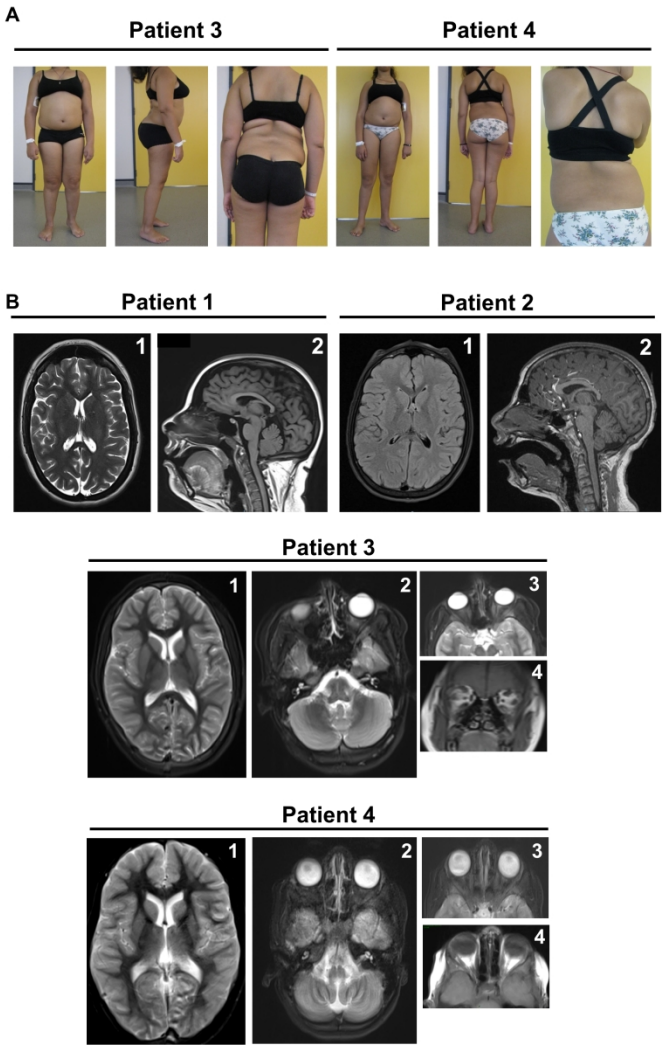

Figure 1: Clinical and brain imaging findings in novel INPP5K-patients. (A) representative photographs of patient 3 and 4 showing severe hyperlordosis. (B) Brain MRI of patients 1-4 showing no brain abnormalities in patients 1, 3 and 4 but a mild cerebellar atrophy in patient 2. Size of oculomotor muscles appears normal in patients 3 & 4 and lenses have obviously been removed with vacuity of the eyes in patient 3 whereas in patient 4 the lenses have not been removed and are well visible within the eye-balls. 1-lateral view; 2-overhead view; 3and 4-ocular view

190x338mm (300 x 300 DPI)

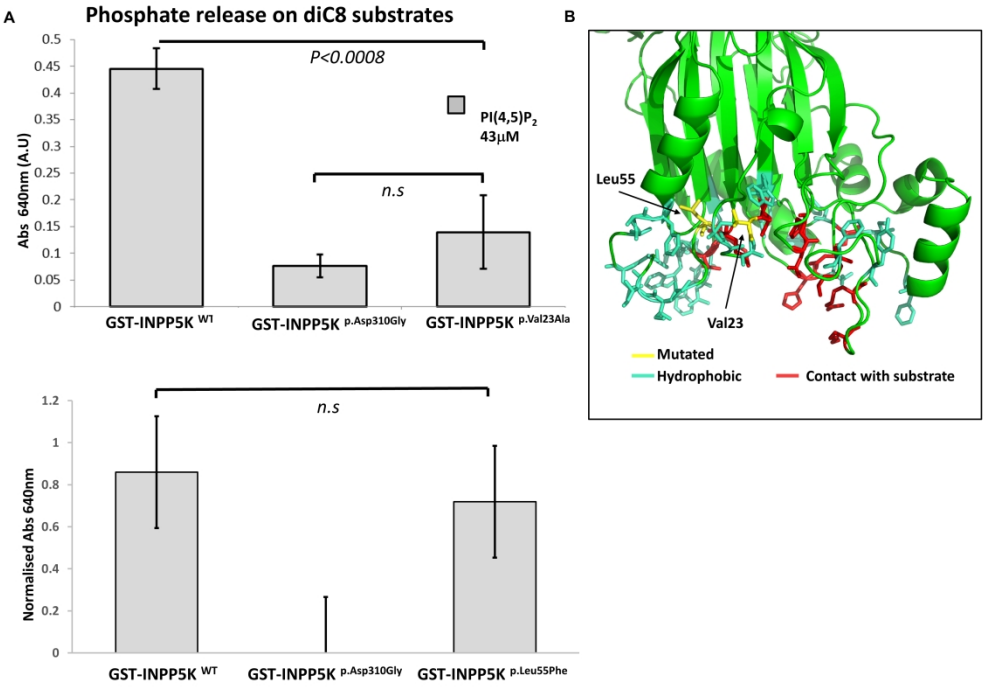

Figure 2. Enzymatic activity of novel missense mutation in INPP5K. (A) Quantification of enzymatic activity of novel missense mutants of INPP5K. GST-INPP5K was bacterially expressed and purified and exposed to the water soluble substrate PI(4,5)P2 diC8, Phosphate released by hydrolysis of PI(4,5)P2 was measured by malachite assay, and the engineered catalytic null mutant INPP5KAsp310Gly was included as a negative control. GST-INPP5KVal23Met has significantly compromised enzymatic activity in this assay (n=3 per condition, t-test), whereas GST-INPP5KLeu55Phe retains near- wildtype levels of activity against water soluble substrate (n=4 wells per condition, t-test). (B) Predicted structure of the INPP5K catalytic domain, modelled using Phyre2 (Kelley et al., 2015). Val23 (yellow) is in the catalytic pocket of the enzyme (red), whereas Leu55 is an internal residue close to a predicted hydrophobic finger (hydrophobic residues coloured blue), which in the enzyme OCRL is thought to assist in associating the catalytic domain with highly curved membranes.

355x266mm (300 x 300 DPI)

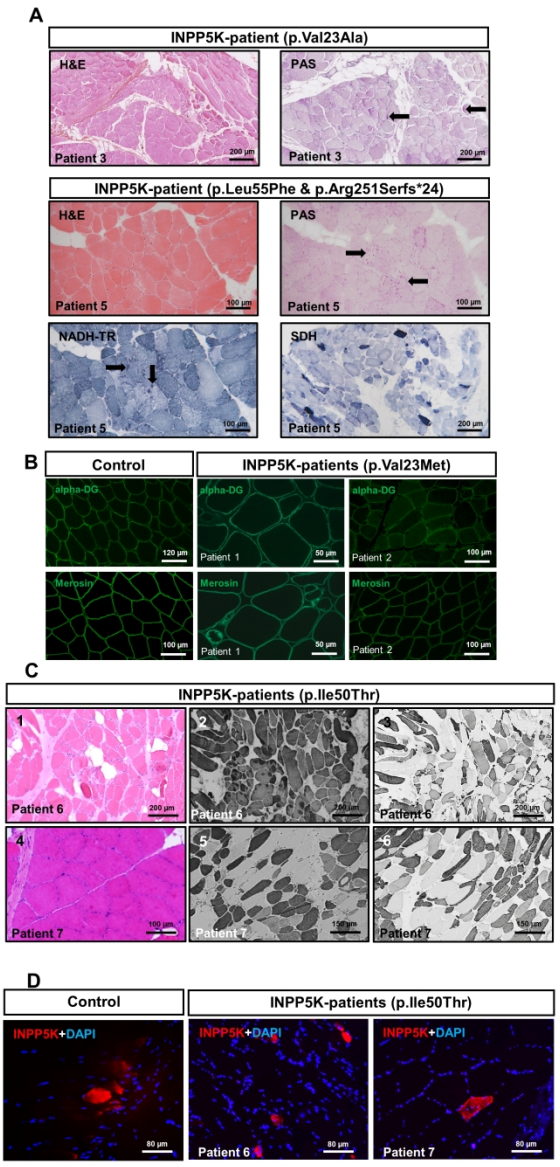

Figure 3: Muscle biopsy findings in INPP5K-patients. (A) Representative histological findings in two (patient 3 & 5) of the five novel INPP5K patients include variation in fiber size, rounding of fibers, increased endomysial collagen and some degree of fatty degeneration as well as focal increase of glycogen as measured by periodic acid-Schiff (PAS) staining in some fibers (black arrows) and focal increase of mitochondria in a proportion of fibers as measured by nicotinamidadenindinucleotide tetrazolium reductase (NADH-TR) reaction (black arrows). Moreover, high oxidative activity is indicated in a proportion of fibers by succinic dehydrogenase (SDH) reaction. (B) Immunofluorescence-based analyses of alpha-dystroglycan and merosin (shown for patients 1 & 2) did not show changes which would accord with a vulnerability of both proteins upon the loss of functional INPP5K.

190x338mm (300 x 300 DPI)

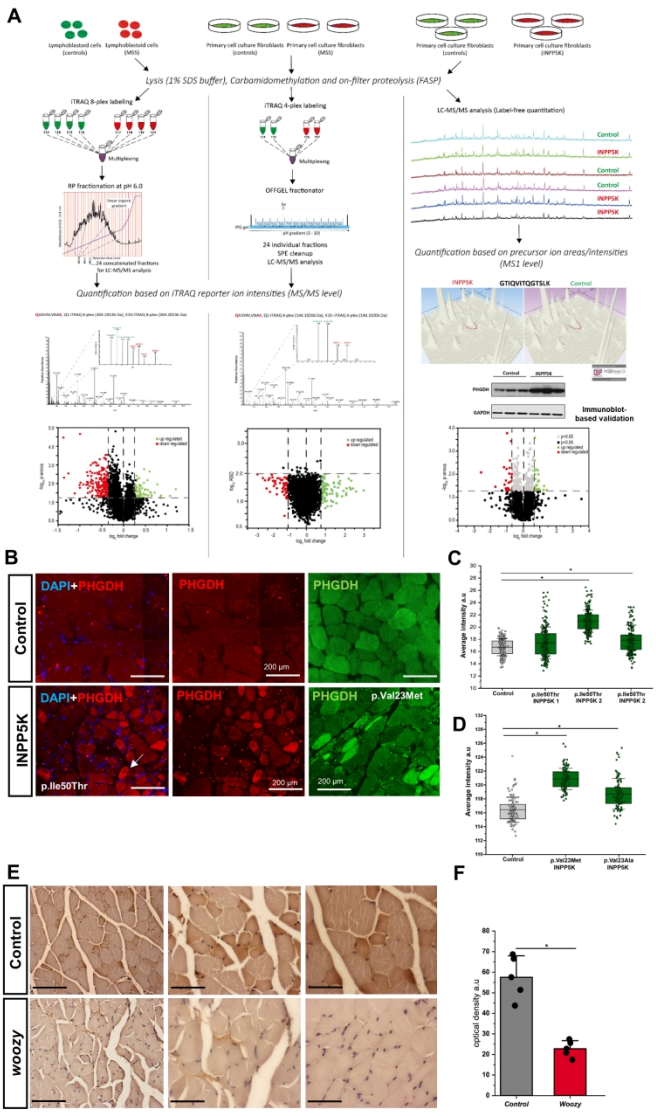

Figure 4: Workflow depicting our protein studies on fibroblasts derived from MSS- and INPP5K-patients. (A) For MSS-patients, immortalized lymphoblastoid cells and primary fibroblasts have been used for iTRAQ-labelling and subsequent peptide-fractionation followed by LC-MS/MS analyses (left and middle column). For primary fibroblast cells derived from INPP5K-patients (all with p.Ile50Thr mutation), label-free protemic profiling was carried out (right column). In all three experiments, as shown by the precursor and reporter ion intensities of the respective experiments (exemplified by the unique peptides of PHGDH i.e. GTIQVITQGTSLK in label-free and QADVNLVNAK in labelling approaches, respectively), PHGDH was altered in abundance: in SIL1-patient derived cells, a statistically significant decrease could be detected whereas in INPP5K-patient derived fibroblasts, a statistically significant increase could be identified. This increase in INPP5K fibroblasts was also confirmed by immunoblotting. The volcano plots highlight our overall proteomic findings: each red and green dot represents a protein altered with a p-Anova ≥ 0.05. (B) Representative PHGDH-staining in a muscle biopsy specimen of a control subject (upper panel) and of a INPP5K-patient harbouring the p.Ile50Thr and p.Val23Met mutation (lower panel) showing an increase of PHGDH in a proportion of diseased muscle fibres. Scale bars: 200□m. (C and D) Box plot depicting the florescence data

points measured in two controls and three (p.Ile50Thr) respectively two (p.Val23Met and p.Val23Ala) patients. The central band represents the median, the lower and upper hinges correspond to the first and third quartiles (25 and 75%) while the whiskers extend to the highest and lowest points within the data (1.5× the inter-quartile range). Results were observed in one (n=1) independent experiments (due to the limited amount of sample). Statistical analysis unpaired Student's t-test was employed where *P ≤ 0.05 was considered statistically significant. (E) Immunohistochemistry analysis of PHGDH on paraffin sections from paraformaldehyde-fixed quadriceps muscle specimens of 26-week-old wild type and three woozy mouse muscle. Scale bars: 22 □m (F) Optical Density (OD) determination of (F) where graph show the results of our three independent experiments resulted from the analysis of three controls and three woozy mice. Data represent mean ± SEM, statistical analysis unpaired Student's t-test was employed where *P ≤ 0.05 was considered statistically significant. Similar results were observed in at least three (n=3) independent experiments.

190x338mm (300 x 300 DPI)

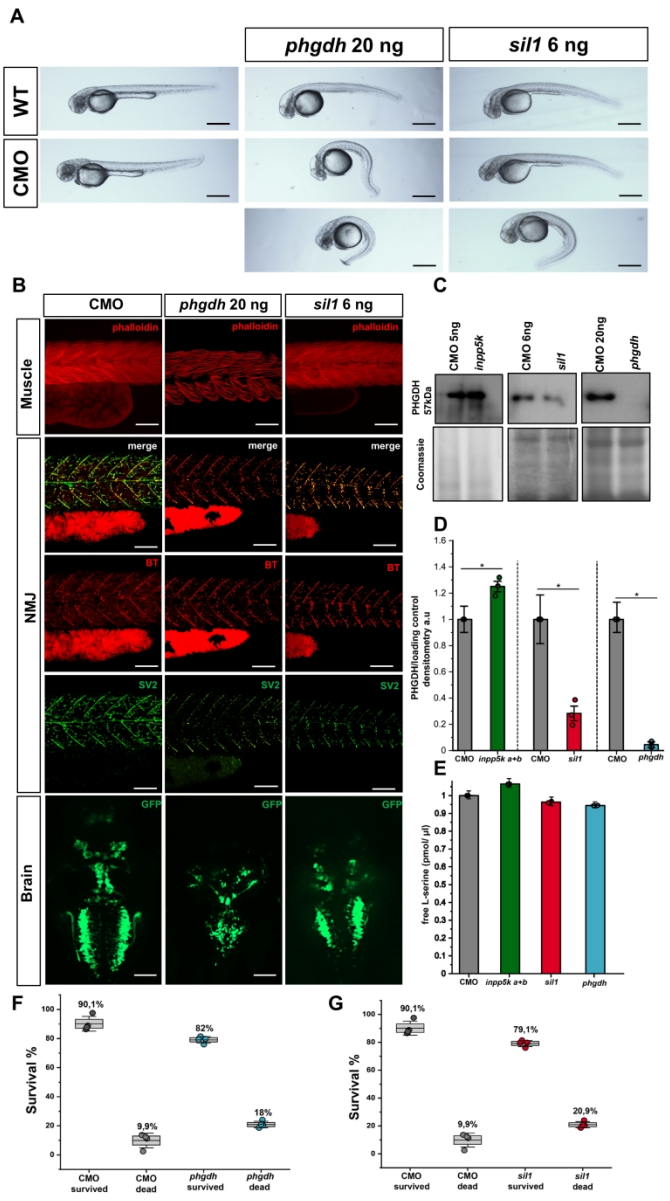

Figure 5: Phenotyping of phgdh- and sil1-morphants. (A) Morpholino-based depletion of phgdh and sil1 in 48 hpf zebrafish resulted in abnormal curvature of the tails of both models compared to wildtype (WT) and control-morpholino (CMO) injected ones. (B) Immunofluorescence-based studies of tissue morphologies revealed disintegration of muscle fibres visualized by phalloidin staining (first lane), abnormal patterning of the pre-synaptic NMJs visualized by reduced SV2-immunoreactivity (lanes 2-4) and abnormal development of the brain affecting the cranial nerves (lane 5) in both fish models. Scale bars: 50 □m. Regarding brain abnormalities, in phgdh-morphants nerves Va, Vp, VI, VII, X and in sil1-morphants nerves III, IV, VI, VII and X are vulnerable to the loss of the respective protein expression. Scale bars: 100 □m. Similar results were observed in at least four (n=4) independent experiments. (C) Western Blot- studies of PHGDH protein level in the three fish models revealed a slight increase in whole protein extracts of inpp5k-morphants but a considerable decrease in the sil1-morphants as well as in the phgdh-morphants. (D) Decrease of the PHGDH protein in the phgdh-morphants reflects the successful morpholino-based depletion of the expression of the corresponding gene as also depicted quantitatively. Data represent mean ± SEM, statistical analysis unpaired Student's t-test was employed where *P ≤ 0.05 was considered statistically significant. Similar

results were observed in at least three (n=3) independent results. (E) Free L-serine analysis in whole embryos at 48 hpf by liquid chromatography. Results accord with the PHGDH expression in zebrafish. Data represent mean ± SEM, statistical analysis unpaired Student's t-test was employed where *P ≤ 0.05 was considered statistically significant. Similar results were observed in at least two (n=2) independent experiments due to the high amount of embryos needed for this analysis. (F and G) Depletion of phgdh and sil2 is also associated with reduced survival of the fish at 48 hpf. The central band represents the median, the lower and upper hinges correspond to the first and third quartiles (25 and 75%) while the whiskers extend to the highest and lowest points within the data (1.5× the inter-quartile range). Statistical analysis unpaired Student's t-test was employed where *P ≤ 0.05 was considered statistically significant. Similar results were observed in at least four (n=4) independent experiments.

190x338mm (300 x 300 DPI)

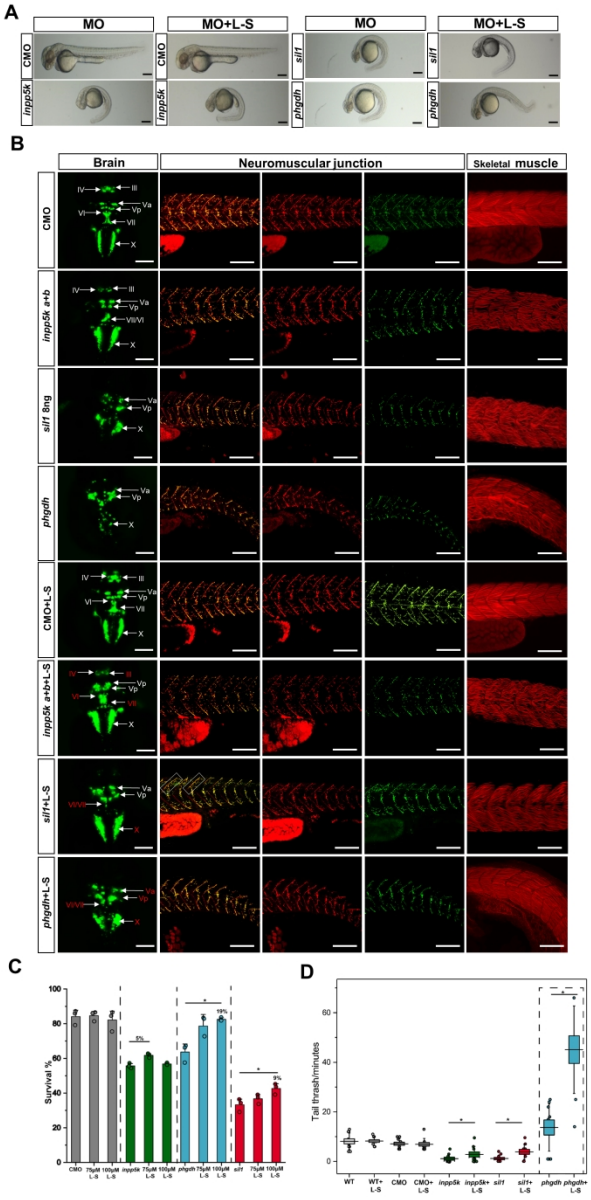

Figure 6: L-serine treatment studies in phgdh-, sil1- and inpp5k-morphants: (A) Study of the effect of L-S treatment (100 µM) on the phenotype of the fish did not reveal changes on the curvature of the tail in the inpp5k- and sil1-morphants, whereas a slight beneficial effect could be observed in the phgdh-morphants, 30 fish were analyzed per condition. Scale bars: 500 □m (B) Results of immunofluorescence-based studies of L-S treatment (100 µM) in tissues vulnerable against the depletion of inpp5k-, sil1- and phgdh-expression. A slight amelioration of muscle fibre integrity can only be identified in the phgdh-morphants but not in the two other models. A minimum of 10 fish were analyzed per condition. Scale bars: 50 µm. In contrast, the pre-synaptic phenotype was ameliorated in the sil1- as well as in the phgdh-morphants, as exemplified by an increase of SV2-immunoreactivity (inpp5k-morphants did not show an NMJ-phenotype per se). A minimum of 10 fish were analyzed per condition. Scale bars: 50 µm. In addition, GFP-fluorescence intensity suggests that the cranial nerves III, IV, VI and VII improved in inpp5k-morphants. sil1-morphants showed a phenotype amelioration of the nerves VI, VII as well as X and the phgdh-morphants of nerves Va, Vp, VI, VII and X after treatment based on increased GFP-fluorescence intensity. A minimum of 10 fish were analyzed per condition. Scale bars: 100 µm.

190x338mm (300 x 300 DPI)

Patient	1	2	3	4	5	6
Sex	Female	Male	Female	Female	Female	Female
Age at molecular diagnosis	25 years	15 years	11 years	13 years	51 years	10 years
Origin	Italy	Italy	Reunion Island	Reunion Island	Italy	Italy
INPP5K variant	p.Val23Met	p.Val23Met	p.Val23Ala	p.Val23Ala	p.Leu55Phe and p.Arg251Serfs*24	p.Val23Met
Initial presenting symptom	Cognitive delay (early infancy)	Mild cognitive and motor delay (early infancy)	Muscle weakness (early childhood)	Muscle weakness (early childhood	Muscle weakness (early childhood)	Muscle weakness
Cataracts (at age)	Yes (?)	Yes (3 years)	Yes (4 years)	No	No	Yes (3 years)
Hypotonia	?	?	?	?	Not reported	Yes
Delayed motor milestones	No	Yes (mild)	?	?	No	Yes (mild)
Muscle weakness/ atrophy	P > D (10 y), pseudohypertrophy of calves and hypotrophy of quadriceps (22 y)	P > D with positive Gower's sign	-	-	Proximal > distal	proximal muscle weakness with a positive Gowers
CK	x2	x3	x5	x5	x 10^{-12}	?
Biopsy findings	Dystrophic changes, variable fibre diameter, mildly increased perimysial connective tissue, centrally located myonuclei	Myopathic changes characterized by myofiber size variability, and internalized myonuclei	Dystrophic pattern	Dystrophic pattern	Myopathy with glycogen accumulation	Dystrophic pattern
Intellectual disability	Moderate	?	?	?	Mild	Mild
Brain anomaly	Not present	Mild cerebellar atrophy	Not present	Not present	Not present	Not present
Other findings	Microcephaly and short stature (below the 3rd centile), severe hyperlordosis	Clubfoot correction	-	-	Myalgias, short stature, sensory axonal neuropathy	Short stature, mild foot deformity and reduced mineral bone density

Table 1 Clinical features of individuals with bi-allelic *INPP5K* mutations

CK = serum creatine kinase; P > D = proximal muscles more severely affected than distal muscles.

Symptoms	*SIL1* patients	*INPP5K* patients	*PHGDH* patients
Vulnerability of skeletal muscle	Progressive vacuolar myopathy	Congenital muscular dystrophy	Not described
Cataracts	Congenital or infantile	Congenital	Congenital
Intellectual disability	Present (varying degree)	Present (mild)	Present
Ataxia	Cerebellar ataxia	First case of cerebellar atrophy is described in this study	Cerebellar ataxia
Neuropathy	One described case with motorneuropathy and axonal vulnerability and two cases with axonal degeneration on the ultra-morphological level	First case of neuropathy is described in this study	Axonal
Microcephaly	Present	Not described	Present

Table 2 Clinical comparison of MSS (SIL1 patients), and *INPP5K* mutation- and *PHGDH* mutation-associated phenotypes